8-2015

Upper Plate Reverse Fault Reactivation and the Unclamping of the Megathrust During the 2014 Northern Chile Earthquake Sequence

Gabriel González
Universidad Católica del Norte

Pablo Salazar
Universidad Católica del Norte

John P. Loveless
Smith College, jloveles@smith.edu

Richard W. Allmendinger
Cornell University

Felipe Aron
Stanford University

See next page for additional authors

Recommended Citation

González, Gabriel; Salazar, Pablo; Loveless, John P.; Allmendinger, Richard W.; Aron, Felipe; and Shrivastava, Mahesh, "Upper Plate Reverse Fault Reactivation and the Unclamping of the Megathrust During the 2014 Northern Chile Earthquake Sequence" (2015). Geosciences: Faculty Publications, Smith College, Northampton, MA.
https://scholarworks.smith.edu/geo_facpubs/22

Authors
Gabriel González, Pablo Salazar, John P. Loveless, Richard W. Allmendinger, Felipe Aron, and Mahesh Shrivastava

Publisher: GSA
Journal: GEOL: Geology
DOI:10.1130/G36703.1

Upper plate reverse fault reactivation and the unclamping of the megathrust during the 2014 Northern Chile earthquake sequence

Gabriel González[1], Pablo Salazar[1], John P. Loveless[2], Richard W. Allmendinger[3], Felipe Aron[4,5], and Mahesh Shrivastava[1]

[1]*National Research Center for Integrated Natural Disaster Management, Universidad Católica del Norte, Avenida Angamos 0610, Antofagasta, Chile*

[2]*Department of Geosciences, Smith College, Northampton, Massachusetts 01063, USA*

[3]*Department of Earth and Atmospheric Sciences, Cornell University, Ithaca, New York 14853, USA*

[4]*Department of Geological Sciences, Stanford University, Stanford, California 94305, USA*

[5]*Departamento de Ingeniería Estructural y Geotécnica, Pontificia Universidad Católica de Chile, Vicuña Mackenna 4860, Macul, Santiago, Chile*

ABSTRACT

After 137 years without a great earthquake, the central portion of the southern Perú-northern Chile subduction zone experienced the M_W 8.1 Pisagua event on April 1, 2014. This megathrust earthquake was preceded most notably by more than two weeks of foreshock activity migrating ~3.5 km/day toward the mainshock hypocenter. This foreshock sequence was triggered by a M_W 6.7 earthquake on a reverse fault in the upper plate that strikes at a high angle to the trench, similar to well-documented reverse faults onshore. These margin-oblique reverse faults accommodate north-south shortening resulting from subduction across a plate boundary that is curved in map view. Reverse slip on the crustal fault unclamped the subduction interface, precipitating the subsequent megathrust foreshock activity that culminated in the great Pisagua

earthquake. The combination of crustal reverse faults and a curved subduction margin also occurs in Cascadia and northeastern Japan, indicating two additional localities where great megathrust earthquakes may be triggered by upper plate fault activity.

INTRODUCTION

Two recent great subduction earthquakes (2010 M_W 8.8 Maule and 2011 M_W 9.1 Tohoku-Oki) and associated upper plate aftershocks have underscored the importance of crustal faulting triggered by megathrust events (Aron et al., 2013; Toda and Tsutsumi, 2013). However, the possibility that a foreshock on an upper plate fault might contribute to triggering a subduction great earthquake has never been clearly documented. On April 1, 2014, the M_W 8.1 Pisagua earthquake broke the central section of the Iquique Gap, a segment of the Nazca-South America subduction zone that last ruptured in an estimated M_W 8.7–8.9 event in 1877 (e.g., Comte and Pardo, 1991). The 2014 earthquake was preceded by 13 months of seismic activity (Schurr et al., 2014), which intensified following the March 16 M_w 6.7 earthquake offshore the town of Pisagua. Over the next 16 days, foreshocks progressively migrated toward the position of the M_w 8.1 mainshock.

The M_W 6.7 earthquake, the largest foreshock (Hayes et al., 2014; Schurr et al., 2014), is significant for two reasons: its location in the upper plate and the orientation of the nodal planes, which deviate significantly from the megathrust strike, as given in the USGS Slab1.0 model (Hayes et al., 2012; Ruiz et al., 2014). Yet, to date, the role that the M_W 6.7 played in the intensification of foreshock activity has not been discussed in detail in the analyses of the PES (e.g., Yagi et al., 2014, Lay et al., 2014, Kato and Nakawaga, 2014, Ruiz et al., 2014, Hayes et al., 2014; Schurr et al., 2014). Based on event relocations, analysis of available focal mechanisms, and static stress change calculations, we illustrate how this major upper plate reverse faulting earthquake was the principal, if not the initial, trigger of subsequent foreshock activity on the megathrust that led to the M_W 8.1 mainshock. We use geologic and seismic data to illustrate that margin-oblique, upper plate reverse faulting is widespread in the northern Chilean forearc, likely related to the bending of the orocline (Allmendinger et al., 2005), and in this case led to a great earthquake on the megathrust.

MARGIN PARALLEL SHORTENING

Within a 250 km-long segment (19.2º–21.6ºS), numerous kilometer-scale, margin-oblique active reverse faults cut the forearc overlying the concave-seaward portion of the Andean subduction zone (Fig. 1; Allmendinger et al., 2005). At at least four sites along the coastline, reverse faults offset Quaternary marine terraces (Fig. DR1) and cumulative vertical offset of Mio-Pliocene surfaces by single reverse faults reaches 500 m. Strikes of these reverse faults vary between 065º and 135º (Fig. 1j), and slickenlines are oriented mainly subparallel to the dip direction, indicating the prevalence of reverse motion. Using fault plane and slickenline orientations, we estimate a mean shortening axis (P-axis) for these faults as subhorizontal, trending 173º, and a subvertical extension axis (T-axis) (Fig. 1i). Kinematic data for single structures show moderate scatter of P and T axes, controlled mainly by variation in fault strike.

Between March 2010 and March 2012, a local seismological network of 21 short period stations was installed in the Coastal Cordillera and Precordillera around 21ºS with the aim of characterizing upper plate seismicity in the forearc (Bloch et al., 2014). We recorded 31 $0.6 \leq M_W \leq 2.7$ crustal earthquakes with kinematics similar to those of the faults preserved in the geologic record (Fig. 1g): reverse faulting on margin-oblique planes. This microseismic activity spans shallow depths (6.9 km) to the plate interface at ~50 km depth, indicating that margin-oblique reverse faults are active throughout the entire crust.

THE PISAGUA EARTHQUAKE FORESHOCK SEQUENCE

The April 1 M_w 8.1 Pisagua mainshock and its foreshocks are collectively termed the Pisagua earthquake sequence (PES). Schurr et al. (2014) showed a slowly decreasing seismicity rate before the largest foreshock. The time series of cumulative seismic moment release reveals that three earthquake clusters punctuated the background seismicity since at least ten months before the mainshock. The pattern of decreasing of seismicity rate was interrupted immediately after the M_w 6.7 event, which represents the peak of foreshock activity (Fig. 2a).

We relocated $M_w > 4$ foreshocks that occurred between March 16 and March 31 using the codes NonLinLoc (Lomax et al., 2000) and HypoDD (Waldhauser and Ellsworth, 2000). The relocation reveals clustering of seismicity at two depths: 1) < 20 km (including the M_w 6.7 earthquake), inside the upper plate, and 2) on the interplate contact (Fig. 2b). Just a few hours after the M_W 6.7 event, the majority of seismicity migrated to the plate interface, but sporadic upper plate events also took place until at least April 15. Our relocated distribution of foreshock latitudes shows that after the M_w 6.7 event, seismicity on the plate interface migrated northward parallel to slab strike at ~3.3 ± 0.33 km/day and down dip at ~1.3 ± 0.2 km/day toward the position of the April 1 M_W 8.1 event (Fig. DR2). The total migration distance of foreshocks is ~49 km along a line of trend and plunge 004º, 08º.

FOCAL MECHANISM ANALYSIS AND REGIONAL STRUCTURES

Focal mechanisms for the M_W 6.7 earthquake were reported by the USGS, Global CMT, and GEOFON-GFZ agencies (Table DR1). We derived our own focal mechanism based on moment tensor inversion from waveform analysis. All available focal mechanisms feature two nodal planes oriented obliquely to the local 341° strike of the megathrust. The average orientation of the low angle, north-dipping nodal plane is 285°, 25°N and the high-angle, south-dipping nodal plane is oriented 128°, 68°W, with a P-axis of trend and plunge 213º, 27º (Fig. 1a). The 64 summed moment tensors available for the vast majority of foreshocks after the M_W 6.7 yield a composite focal mechanism with the low-angle plane oriented 342°, 16°E, which is within 5° of the local strike and dip of the subduction zone from Slab 1.0.

Scaling laws of Wells and Coppersmith (1994) suggest a source fault 36 km along strike and 14 km down dip for the M_W 6.7 upper plate event. The small dimensions of the reactivated fault preclude a direct connection to any mapped onshore structures. However, the orientations of the two nodal planes of the M_w 6.7 event are consistent with the strikes of reverse faults onshore (Fig. 1i, 1j), as well as nodal planes of past crustal seismicity (Fig. 1e–g). Therefore we suggest that the M_w 6.7 earthquake may have reactivated a continuation of a structure similar to those documented onshore.

STATIC STRESS CHANGE ANALYSIS

We use static stress change calculations to explore the relationship between the upper plate M_W 6.7 earthquake and seismicity on the subduction megathrust. First, we calculated (using algorithms of Meade, 2007) the cumulative Coulomb stress change (CSC) imparted on the upper plate fault by the July 2013 and January 2014 earthquake clusters identified by Schurr et al. (2014) and found that they induced a very small CSC (< 0.003 bars, or 300 Pa).

Subsequently, we focused on the possibility that the M_W 6.7 event triggered seismicity on the plate boundary that ultimately migrated toward the M_W 8.1 earthquake. We calculated the distribution of static CSC induced on the subduction interface by the M_W 6.7 earthquake and compared that to our relocations of subsequent megathrust foreshocks. We modeled each nodal plane of the M_W 6.7 event as a rectangular source fault using empirical scaling laws (Wells and Coppersmith, 1994) and using our derived location and the USGS Mww focal mechanism (Table

DR1). The regions of positive CSC up to ~5 bars (0.5 MPa), defined with shear stress change in the local up-dip direction, generated by the north-dipping nodal plane contain 51% of the NonLinLoc-located aftershocks in the first 24 h after the M_W 6.7 event, while positive CSC zones calculated using the south-dipping plane contain 36% of these events (Figs. 3, DR8). However, regions of positive normal stress (unclamping) on the megathrust contain up to 84% (for the north-dipping plane; 74% for the south-dipping plane) of these events, suggesting that reverse slip on either plane unclamped the megathrust (Figs. 3a and DR6) and facilitated the subsequent megathrust foreshocks given the prevalence of up-dip shear stress accumulated during the preceding interseismic period. The January 2014 cluster of foreshocks that occurred before the M_W 6.7 earthquake (Schurr et al., 2014) also induced CSC on the megathrust of magnitude comparable to that of the upper plate event, localized around the small cluster near 20.2ºS (Fig. 3). Positive CSC induced by all megathrust events between March 16 and March 31 migrated northward and downdip along the megathrust, primarily reflecting increased up-dip shear stress induced by the foreshock sequence (Figs. 3c, DR7). The hypocenter of the M_w 8.1 Pisagua earthquake was in a region of positive CSC, just downdip from a cluster of foreshocks.

DISCUSSION

Geologic and seismic data show that the area around the PES is characterized by margin-parallel upper plate shortening, which is expressed on short timescales in seismic records and on neotectonic timescales in the geology. This deformation regime is consistent with the obliquity of the nodal planes of the upper plate M_w 6.7 foreshock relative to the strike of the megathrust, with remarkable similarity between the kinematics inferred for this earthquake and those of the onshore seismicity and geologic fault plane analysis (Fig. 1). In particular, the P-axis of the M_w 6.7 event is similar to the P-axes estimated from geological structures and upper plate earthquakes previously detected in the area (Fig. 1i). Therefore we conclude that the M_w 6.7 event represents the reactivation of one of the trench-oblique upper plate reverse faults common in this part of the forearc.

Recent work has suggested that during the PES, the megathrust was gradually unlocked by a propagation of long-term precursory events (Schurr et al., 2014). Our stress change analysis shows that the March 16 M_W 6.7 foreshock unclamped the megathrust, triggering the subsequent migrating sequence of foreshocks. Similar analysis indicates that the foreshocks before the middle of March did not transfer significant stress from the megathrust to the upper plate fault. Additionally, the stress perturbation on the megathrust due to earthquake clusters prior to mid-March was localized compared to that promoted by the M_W 6.7 earthquake and subsequent events (Fig. 3). Therefore, we conclude that the occurrence of the M_W 6.7 earthquake primarily represents accommodation of trench-parallel shortening, and that the final conditioning of the megathrust in generating the great M_W 8.1 event was strongly influenced by the upper plate deformation regime. A key requirement of this process is the synchronicity of the earthquake cycles on the upper plate fault and the megathrust. If the megathrust had not yet reached a mature state in its interseismic period, then the stress conditions on it may not have been suitable to produce a major rupture under the loading increment imposed by the upper plate faulting event. In the Iquique Gap, 137 years had elapsed since the last great earthquake, representing a complete interseismic period (e.g., Comte and Pardo, 1991).

The concave-seaward northern Chile-southern Perú margin is similar in shape to the northern Cascadia and northeast Japan Trench subduction zones, and in each, upper plate reverse faults that strike nearly orthogonal to the plate boundary are present (e.g., Johnson et al., 2004; Kusunoki and Kimura, 1998). Concave-seaward segments of subduction zones can experience interseismic shortening perpendicular to the direction of convergence, as velocity in that direction decreases toward the apex of margin curvature (Bevis et al., 2001), and this shortening may be enhanced by spatially heterogeneous interplate coupling (Rosenau et al., 2009). McCaffrey et al. (2013) show contractional interseismic strain in the Cascadia forearc from the Olympic Peninsula to the Puget Lowlands, with shortening in the direction of plate convergence (ENE) but also in the perpendicular direction. In Hokkiado, Japan, Loveless and Meade (2010) estimate reverse slip on the margin-perpendicular Hidaka Fold-and-Thrust Belt based on analysis of interseismic GPS velocities. Thus in each of these cases, margin-oblique reverse faults are loaded by subduction zone interseismic processes, yielding the possibility of megathrust activity triggered by seismicity on upper plate structures. This mechanism, which we have documented here for the PES case, encourages further study of crustal fault recurrence intervals, particularly in Cascadia where 315 years have passed since the great M_w 9.0 earthquake of 1700 and the seismic risk posed by both megathrust and upper plate earthquakes is large.

CONCLUSIONS

We suggest that the April 1, 2014 M_w 8.1 Pisagua subduction earthquake was mostly triggered by the March 16 M_w 6.7 foreshock on an upper plate reverse fault southwest of the mainshock epicenter. We show that static unclamping of the megathrust produced by the upper plate earthquake is likely the dominant mechanism that led to the subsequent foreshock-mainshock sequence. Following this main precursory event, progressive stressing of the subduction interface by the northeastward migration of additional foreshocks on the megathrust culminated in the partial rupture of the Iquique Gap. The recent experience in northern Chile indicates that, when assessing seismic hazard, earthquakes on upper plate faults should be taken into consideration, not only because of the locally high intensity shaking that they can produce, but also as possible triggering mechanisms for great earthquakes on the subduction zone interface.

ACKNOWLEDGMENTS

We thank James Spotila, Onno Oncken, Brian Atwater, Chris Goldfinger, and two anonymous readers for helpful reviews. This research was supported by CONICYT/ FONDAP grant 15110017. Allmendinger is grateful for support from NSF Grants EAR-1443410, EAR-1019252, and EAR-05107852. Aron acknowledges support from CONICYT Beca Chile and NSF grant EAR-1118678.

REFERENCES CITED

Allmendinger, R., González, G., Yu, J., Hoke, G., and Isacks, B., 2005, Trench parallel shortening in the Northern Chilean Forearc: Tectonic and climatic implications: Geological Society of America Bulletin, v. 117, no. 1–2, p. 89–104, doi:10.1130/B25505.1.

Aron, F., Allmendinger, R. W., Cembrano, J., González, G., and Yáñez, G., 2013, Permanent fore-arc extension and seismic segmentation: Insights from the 2010 Maule earthquake, Chile: Journal of Geophysical Research, v. 118, no. 2, p. 724-739. doi:10.1029/2012JB009339.

Bevis, M., Kendrick, E., Smalley, R., Brooks, B., Allmendinger, R.W., and Isacks, B.L., 2001, On the strength of interplate coupling and the rate of backarc convergence in the central Andes: An analysis of the interseismic velocity field: Geochemistry Geophysics Geosystems, v. G3, no. 2, doi:10.1029/2001GC000198.

Bloch, W., Kummerow, J., Salazar, P., Wigger, P., and Shapiro, S., 2014, High-resolution image of the North Chilean subduction zone: Seismicity, reflectivity and fluids: Geophysical Journal International, v. 197, no. 3, p. 1744–1749, doi:10.1093/gji/ggu084.

Comte, D., and Pardo, M., 1991, Reappraisal of great historical earthquakes in the northern Chile and southern Peru seismic gaps: Natural Hazards, v. 4, p. 23–44, doi:10.1007/BF00126557.

Hayes, G.P., Wald, D.J., and Johnson, R.L., 2012, Slab1.0: A three- dimensional model of global subduction zone geometries: Journal of Geophysical Research, v. 117, no. B1, B01302, doi:10.1029/2011JB008524.

Hayes, G.P., Herman, M.W., Barnhart, W.D., Furlong, K.P., and Riquelme, S., 2014, Benz, H. M., Bergman, E., Barrientos, S., Earle, P.S. and Samsonov, S., 2014, Continuing megathrust earthquake potential in Chile after the 2014 Iquique earthquake: Nature, v. 515, p. 295–298, doi:10.1038/nature13677.

Johnson, S.Y., Blakely, R.J., Stephenson, W.J., Dadisman, S.V., and Fisher, M.A., 2004, Active shortening of the Cascadia forearc and implications for seismic hazards of the Puget Lowland: Tectonics, v. 23, TC1011, doi:10.1029/2003TC001507.

Kato, A., and Nakagawa, S., 2014, Multiple slow-slip events during a foreshock sequence of the 2014, Chile Mw 8.1 earthquake: Geophysical Research Letters, v. 41, p. 5420–5427, doi:10.1002/2014GL061138.

Kusunoki, K., and Kimura, G., 1998, Collision and extrusion at the Kuril-Japan arc junction: Tectonics, v. 17, no. 6, p. 843–858, doi:10.1029/98TC02699.

Lay, T., Yue, H., Brodsky, E., and An, Ch., 2014, The 1 April Iquique, Chile, Mw 8.1 earthquake rupture sequence: Geophysical Research Letters, v. 41, p. 3818–3825, doi:10.1002/2014GL060238.

Lomax, A.J., Virieux, P., Volant, P., Berge, C., 2000, Probabilistic earthquake location in 3D and layered models: Introduction of a Metropolis-Gibbs method and comparison with linear locations, *in* Thurber, C.H., Rabinowitz, N., eds., Advances in Seismic Event Location:

Amsterdam, Springer, p. 101–134.

Loveless, J.P., and Meade, B.J., 2010, Geodetic imaging of plate motions, slip rates, and partitioning of deformation in Japan: Journal of Geophysical Research, v. 115, B02410, doi:10.1029/2008JB006248.

McCaffrey, R., King, R.W., Payne, S.J., and Lancaster, M., 2013, Active tectonics of northwestern U.S. inferred from GPS-derived surface velocities: Journal of Geophysical Research, v. 118, p. 709–723, doi:10.1029/2012JB009473.

Meade, B.J., 2007, Algorithms for the calculation of exact displacements, strains, and stresses for triangular dislocation elements in a uniform elastic half space: Computers & Geosciences, v. 33, p. 1064–1075, doi:10.1016/j.cageo.2006.12.003.

Rosenau, M., Lohrmann, J., and Oncken, O., 2009, Shocks in a box: An analogue model of subduction earthquake cycles with application to seismotectonic forearc evolution: Journal of Geophysical Research, v. 114, B01409, doi:10.1029/2008JB005665

Ruiz, S., Métois, M., Fuenzalida, A., Ruiz, J., Leyton, F., Grandin, R., Vigny, C., Madariaga, R., and Campos, J., 2014, Intense foreshocks and a slow slip event preceded the 2014 Iquique Mw 8.1 earthquake: Science, v. 24, no. 6201, p. 1165–1169, doi:10.1126/science.1256074.

Schurr, B., Asch, G., Hainzl, S., Bedford, J., Hoechner, A., Palo, M., Wang, R., Moreno, M., Bartsch, M., Zhang, Y., Oncken, O., Tilmann, F., and Dahm, T., 2014, Victor, P., Barrientos, S. Vilotte, J.-P., 2014, Gradual unlocking of plate boundary controlled initiation of the 2014 Iquique earthquake: Nature, v. 512, p. 299–302, doi:10.1038/nature13681.

Toda, S., and Tsutsumi, H., 2013, Simultaneous reactivation of two, subparallel, inland normal faults during the Mw 6.6 11 April 2011 Iwaki earthquake triggered by the Mw 9.0 Tohoku-oki, Japan, earthquake: Bulletin of the Seismological Society of America, v. 103, no. 2B, p. 1584–1602, doi:10.1785/0120120281.

Waldhauser, F., and Ellsworth, W.L., 2000, A double-difference earthquake location algorithm: Method and application to the northern Hayward fault, California: Bulletin of the Seismological Society of America, v. 90, p. 1353–1368, doi:10.1785/0120000006.

Wells, D.L., and Coppersmith, K.J., 1994, New empirical relationships among magnitude, rupture length, rupture width, rupture area, and surface displacement: Bulletin of the Seismological Society of America, v. 84, p. 974–1002.

Yagi, Y., Okuwaki, R., Enescu, B., Hirano, S., Yamagami, Y., and Endo, S., and Komoro, T., 2014, Rupture Process of the 2014 Iquique Chile Earthquake in Relation with the Foreshock Activity: Geophysical Research Letters, v. 41, p. 4101–4106, doi:10.1002/2014GL060274.

FIGURE CAPTIONS

Figure 1. Location of the study area (inset) and key seismic and structural features. Bathymetry is shown in shades of blue and purple with the Perú-Chile trench in purple. Hill-shaded topography reveals Neogene east-west fault scarps highlighted with magenta lines. Dashed white lines show depth to the subducted plate, in kilometers, from Slab 1.0 (Hayes et al., 2012). Yellow dots show our locations of Pisagua earthquake sequence events as described in the text. Selected fault plane solutions show the kinematic style of earthquakes: (a) M_W 6.7 foreshock on March 16, 2014; (b) M_W 8.1 mainshock on April 1, 2014; (c, d) two upper plate events from the aftershock sequence on April 7 and 15 that show east-west nodal planes and north-south shortening; (e–h) crustal earthquakes with date of occurrence; (g) forearc events recorded during the local microseismic study between 2010 and 2012. (i) Summary of fault kinematics from measured Neogene faults. Blue dots show P-axes and red T-axes. For comparison, yellow stars

show the moment tensor axes of the M_W 6.7 foreshock (a). Fault plane solutions are constructed by summing and averaging all available moment tensor solutions for each event or data set. (j) Magenta bins (10°) showing the angular distribution of length-weighted strikes of mapped margin-oblique reverse faults. The strikes of the high-angle, south-dipping (128°, 68°W) and low-angle, north dipping (285°, 25°N) nodal planes of the M_W 6.7 upper plate foreshock are depicted by the blue and red lines, respectively.

Figure 2. a) Time series of the Pisagua earthquake sequence (PES) events from January 1, 2013 to April 2014 showing the number events per day. The seismicity rate slowly decreased before the March 16, 2014 M_W 6.7 earthquake but increased after that event. b) Earthquake depth plotted versus longitude, showing PES seismicity projected on a cross section orthogonal to the plate boundary. Two groups can be distinguished: upper plate events in red and interplate earthquakes in blue. Error bars show the uncertainty in location given by the NonLinLoc code, and black and green stars show hypocenters of the M_W 6.7 foreshock and M_W 8.1 mainshock, respectively.

Figure 3. Stress change ($\Delta\sigma$) induced on the plate boundary from the foreshocks to the M_W 8.1 Pisagua earthquake at two different times: a) normal (unclamping positive) and b) Coulomb (unclamping and/or updip shear is positive) stress change due to the March 16 M_W 6.7 upper plate earthquake (the effect of the January 2013 seismic cluster identified by Schurr et al. (2014) is shown near −70.8ºW, −20.2ºS), assuming the shallow north-dipping nodal plane; and c) Coulomb stress change immediately prior to the April 1 mainshock. For the M_W 6.7 event, a rectangular source fault geometry, outlined in yellow with green indicating the shallow edge, was defined using empirical scaling relationships (Wells and Coppersmith, 1994), with our relocated hypocenter at the centroid. Slip was imposed in the rake direction of the USGS Mww

focal mechanism. We resolved stress on the megathrust and used an effective friction coefficient of 0.4. Circles show our NonLinLoc-relocated earthquakes following the M_W 6.7 event (events occurring in the first 24 h only are shown in (a) and (b)), and squares show epicenters of pre-March seismicity (Schurr et al., 2014). The epicenter of the mainshock is shown as a yellow star in (c). Iq, Iquique; Pg, Pisagua.

[1] GSA Data Repository item 2015xxx, xxxxxxxx, is available online at www.geosociety.org/pubs/ft2015.htm, or on request from editing@geosociety.org or Documents Secretary, GSA, P.O. Box 9140, Boulder, CO 80301, USA.

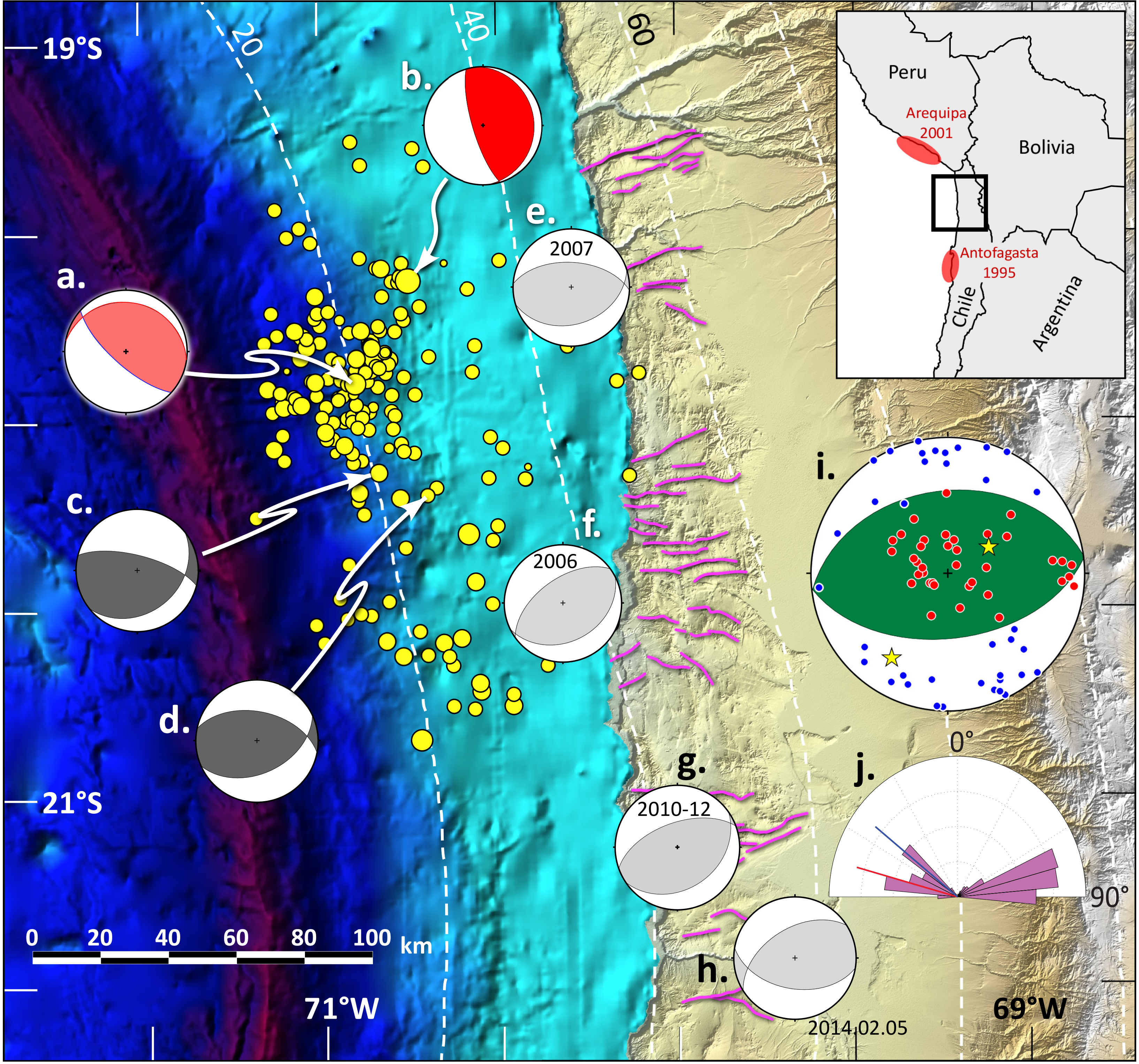
19°S
21°S
71°W
69°W
20
40
60
a.
b.
c.
d.
e.
2007
f.
2006
g.
2010-12
h.
2014.02.05
i.
j.
0°
90°
0
20
40
60
80
100
km
Peru
Arequipa
2001
Bolivia
Antofagasta
1995
Chile
Argentina

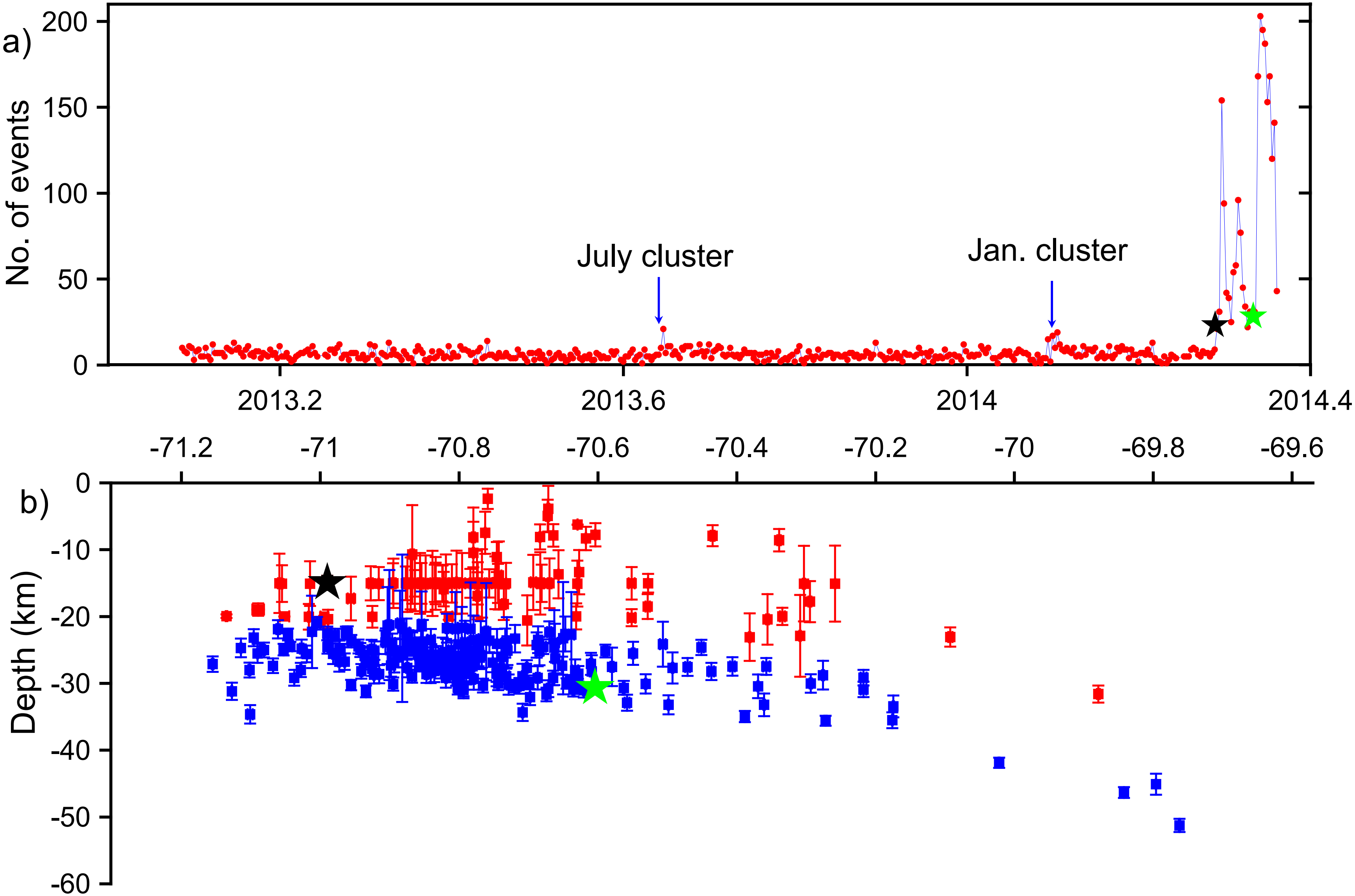
a)
No. of events
200
150
100
50
0
July cluster
Jan. cluster
2013.2
2013.6
2014
2014.4
-71.2
-71
-70.8
-70.6
-70.4
-70.2
-70
-69.8
-69.6
b)
Depth (km)
0
-10
-20
-30
-40
-50
-60

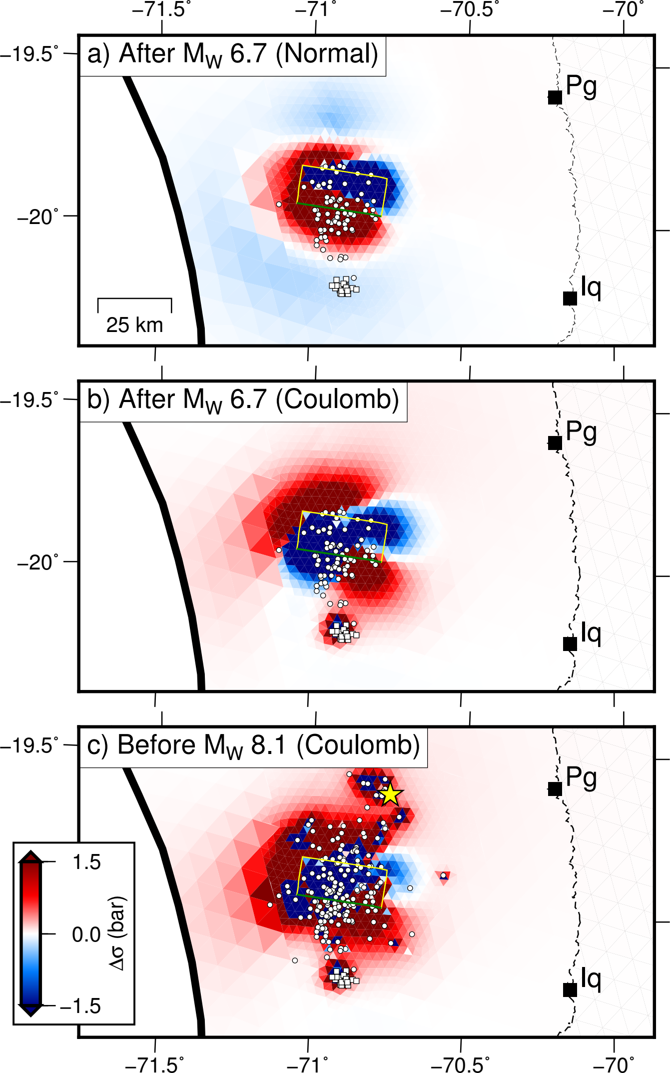
−71.5˚
−71˚
−70.5˚
−70˚
−19.5˚
−20˚
a) After M_W 6.7 (Normal)
Pg
Iq
25 km
b) After M_W 6.7 (Coulomb)
c) Before M_W 8.1 (Coulomb)
1.5
0.0
−1.5
Δσ (bar)